Chapter 10
An Analytical Application: Optimization of a Stirling Engine Based on the Schmidt Analysis and on the Adiabatic Analysis

Alles soll so einfach wie möglich
gemacht werden, aber nicht einfacher.

Everything should be made
as simple as possible, but not simpler.

Albert Einstein

10.1 Introduction

Stirling engines are external combustion engines converting thermal energy into mechanical energy by alternately compressing and expanding a fixed quantity of air or other gas (called the working or operating fluid) at different temperatures [126]. Stirling engines were invented by Robert and James Stirling in 1818. Despite their high efficiency and quiet operation they have not imposed themselves over the Diesel and Otto engines. In recent years interest in Stirling engines has grown, since they are good candidates to become the core component of micro Combined Heat and Power (CHP) units. In this chapter, we discuss an optimization experiment performed on Stirling engines. In particular, optimization algorithms are applied to the Schmidt and to the adiabatic analyses. These are two simple and rather idealized analytical models of the Stirling machine. Before discussing the optimization issue we briefly recall the basic elements of the Stirling cycle, and the Schmidt and the adiabatic analyses.

M. Cavazzuti, *Optimization Methods: From Theory to Design*,
DOI: 10.1007/978-3-642-31187-1_10, © Springer-Verlag Berlin Heidelberg 2013

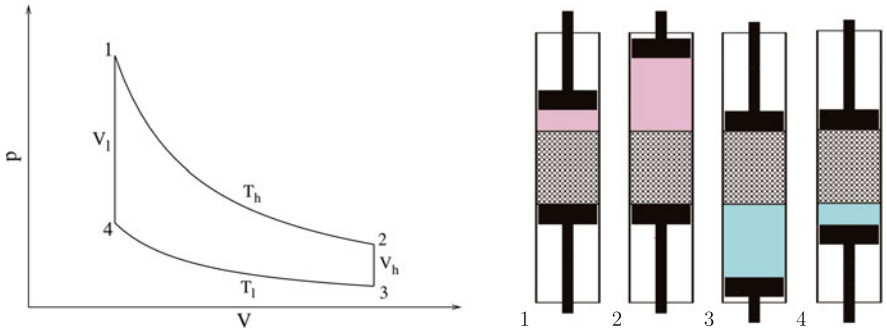

Fig. 10.1 The ideal Stirling cycle

10.1.1 The Stirling Thermodynamic Cycle

Stirling engines are based on the Stirling regenerative thermodynamic cycle which is composed of four thermodynamic transformations:

- an isothermal expansion at high temperature,
- an isochoric regenerative heat removal,
- an isothermal compression at low temperature,
- an isochoric regenerative heat addition.

Since the operating fluid is expanded at high temperature and compressed at low temperature a net conversion of heat into work is attained. The theoretical efficiency of the cycle in case of complete reversibility equals that of the ideal Carnot cycle, as stated by the Reitlinger theorem [127]. An ideal Stirling cycle between the temperatures T_l and T_h ($T_l < T_h$), and between the volumes V_l and V_h ($V_l < V_h$) is represented in Fig. 10.1 and is described by the following equations

$$\begin{array}{ll}
W_{1,2} = \int_1^2 p\mathrm{d}V = MRT_h \ln \frac{V_h}{V_l} > 0 & Q_{1,2} = W_{1,2} = MRT_h \ln \frac{V_h}{V_l} > 0 \\
W_{2,3} = 0 & Q_{2,3} = Mc_v\,(T_l - T_h) < 0 \\
W_{3,4} = MRT_l \ln \frac{V_l}{V_h} < 0 & Q_{3,4} = W_{3,4} = MRT_l \ln \frac{V_l}{V_h} < 0 \\
W_{4,1} = 0 & Q_{4,1} = Mc_v\,(T_h - T_l) = -Q_{2,3} > 0 \\
W_{net} = W_{1,2} - W_{3,4} = MR\,(T_h - T_l) \ln \frac{V_h}{V_l} > 0 & \eta = \frac{W_{net}}{Q_{1,2}} = 1 - \frac{T_l}{T_h} = \eta_{carnot}
\end{array} \tag{10.1}$$

where $W_{m,n}$ and $Q_{m,n}$ respectively are the amount of work and the heat exchanged by the system during the transformation from the status m to the status n, p is the pressure, and M the mass of the operating fluid in the system, R is the specific gas constant, c_v is the specific heat at constant volume of the gas, W_{net} is the net work output, and η the thermodynamic efficiency of the cycle. $Q_{2,3}$ and $Q_{4,1}$ are exchanged regeneratively, thus they are not included into the efficiency equation.

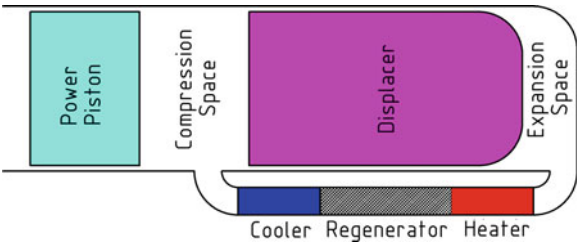

Fig. 10.2 Stirling engine schematic representation

10.1.2 The Schmidt Analysis

Schmidt analysis [128–130] is an ideal isothermal nonlinear model for the simulation of Stirling machines.

The working space of a Stirling machine is composed of:

- a compression space (c),
- a cooler (k),
- a regenerator (r),
- a heater (h),
- an expansion space (e).

Figure 10.2 is a schematic representation of a Stirling machine and its spaces and pistons. The fluid flows back and forth between the expansion and the compression spaces crossing the heater first, then the regenerator, and finally the cooler. The fluid is displaced by the motion of a piston (the displacer) and is compressed and expanded by the motion of another piston (the power piston).

The main assumptions of the Schmidt analysis are:

- constant thermodynamic properties of the operating fluid,
- sinusoidal volume variations in the expansion and the compression spaces due to the pistons motion,

$$V_e(\theta) = V_{d,e} + \frac{V_{sw,e}}{2}(1+\cos\theta), \qquad V_c(\theta) = V_{d,c} + \frac{V_{sw,c}}{2}(1+\cos(\theta-\alpha)) \tag{10.2}$$

- constant volume of the heater, the regenerator, and the cooler,
- constant and uniform temperature equal to T_h in the expansion space and in the heater,
- constant and uniform temperature equal to T_k in the compression space and in the cooler,
- constant and linearly varying temperature in the regenerator between T_k and T_h,
- uniform pressure in the whole working space,

$$p(\theta) = MR\left(\frac{V_c(\theta)}{T_k} + \frac{V_k}{T_k} + \frac{V_r \ln\left(\frac{T_h}{T_k}\right)}{T_h - T_k} + \frac{V_h}{T_h} + \frac{V_e(\theta)}{T_h}\right)^{-1}. \tag{10.3}$$

$\theta \in [0, 2\pi]$ defines the actual phase in the cycle, α the phase lag between the volume variation in the expansion and in the compression space. V stands for the volume, V_d for the dead volume, V_{sw} for the swept volume, p for the pressure, M for the total mass of operating fluid, R for the specific gas constant, T for the thermodynamic temperature. The subscripts e and c stand for expansion and compression spaces respectively, the subscripts h, r, k for the heater, the regenerator, and the cooler. The regenerator mean effective temperature is defined

$$T_r = \frac{T_h - T_k}{\ln \frac{T_h}{T_k}}. \tag{10.4}$$

The following nondimensional parameters are used in the analysis:

- the temperature ratio $\tau = \frac{T_k}{T_h}$,
- the volume ratio $\psi = \frac{V_{sw,c}}{V_{sw,e}}$,
- the regenerator dead volume ratio $x_r = \frac{V_r}{V_{sw,e}}$,
- the hot dead volume ratio $x_h = \frac{V_{d,e}+V_h}{V_{sw,e}}$,
- the cold dead volume ratio $x_k = \frac{V_{d,c}+V_k}{V_{sw,e}}$.

Substituting Eqs. 10.2 into 10.3 yields

$$\frac{MRT_k}{p(\theta) V_{sw,e}} = \frac{\psi}{2}(1 + \cos(\theta - \alpha)) + \frac{\tau}{2}(1 + \cos\theta) + H \tag{10.5}$$

where

$$H = \frac{x_r \tau \ln \frac{1}{\tau}}{1 - \tau} + x_h \tau + x_k \tag{10.6}$$

is the reduced dead volume. The phase angle θ_0 at which the pressure is minimum in the cycle is such that

$$\tan\theta_0 = \frac{\psi \sin\alpha}{\tau + \psi\cos\alpha}. \tag{10.7}$$

Defining

$$K = \frac{2MRT_k}{V_{sw,e}}, \qquad Y = \tau + \psi + 2H \tag{10.8}$$

Equation 10.5 can be written in the form

$$p(\theta) = \frac{K}{Y(1 + \delta\cos(\theta - \theta_0))} \tag{10.9}$$

where

$$\delta = \frac{\sqrt{\tau^2 + \psi^2 + 2\tau\psi\cos\alpha}}{\tau + \psi + 2H} \tag{10.10}$$

is the pressure swing ratio. The mean pressure over the cycle is

$$p_m = \frac{1}{2\pi}\int_0^{2\pi} p\,(\theta)\,\mathrm{d}\theta = \frac{K}{Y\sqrt{1-\delta^2}}. \tag{10.11}$$

The expansion and compression work during one cycle is given by

$$W_e = Q_e = \oint p\,\mathrm{d}V_e = \int_0^{2\pi} p\frac{\mathrm{d}V_e}{\mathrm{d}\theta}\mathrm{d}\theta = \frac{\pi p_m V_{sw,e}\delta\sin\theta_0}{1+\sqrt{1-\delta^2}} \tag{10.12}$$

$$W_c = Q_c = \oint p\,\mathrm{d}V_c = \int_0^{2\pi} p\frac{\mathrm{d}V_c}{\mathrm{d}\theta}\mathrm{d}\theta = \frac{\pi p_m \psi V_{sw,e}\delta\,\sin\,(\theta_0-\alpha)}{1+\sqrt{1-\delta^2}}. \tag{10.13}$$

It follows that the net power output and the efficiency of the cycle are

$$W_{net} = W_e + W_c = \frac{\pi p_m V_{sw,e}\delta\,(1-\tau)\sin\theta_0}{1+\sqrt{1-\delta^2}}, \qquad \eta = 1-\tau = \eta_{carnot}. \tag{10.14}$$

Thus, the Schmidt analysis still yields the ideal Carnot efficiency. The work output depends upon the following parameters: x_r, x_h, x_k, ψ, τ, α, M, R, T_k, $V_{sw,e}$.

W_{net} can be expressed in nondimensional form by dividing by MRT_k or by $p_{max}V_{sw,e}$

$$\bar{W}_{net} = \frac{W_{net}}{MRT_k} = \frac{2\pi\delta\,(1-\tau)\sin\theta_0}{\sqrt{1-\delta^2}\Big(\tau+\psi+2H\Big)\Big(1+\sqrt{1-\delta^2}\Big)} \tag{10.15}$$

$$\tilde{W}_{net} = \frac{W_{net}}{p_{max}V_{sw,tot}} = \frac{\pi\delta\sqrt{1-\delta}\,(1-\tau)\sin\theta_0}{\sqrt{1+\delta}\Big(1+\psi\Big)\Big(1+\sqrt{1-\delta^2}\Big)} \tag{10.16}$$

where $V_{sw,tot} = V_{sw,e} + V_{sw,c}$. The net work output given by the nondimensional Schmidt analysis just depends upon x_r, x_h, x_k, ψ, τ, α. According to the Schmidt analysis, the dead volumes are always reducing the work output, and the smaller is τ the higher is the net work output. Thus, for a given τ value, the optimal values of the parameters are $x_r = x_h = x_k = 0$. From this situation it follows that a meaningful nondimensional optimization would involve just two input variables: ψ and α. However, it must be considered that the optimum configurations also depend upon x_r, x_h, x_k, and τ, since $\bar{W}_{net} = \bar{W}_{net}\,(\tau, \psi, \alpha, H)$, and $\tilde{W}_{net} = \tilde{W}_{net}\,(\tau, \psi, \alpha, H)$. In fact, all the terms in Eqs. 10.15 and 10.16 can be written as functions of τ, ψ, α,

H, and H depends upon x_r, x_h, x_k. Figure 10.3 shows the nondimensional net work output as a function of ψ and α.

In real engines, actually, there is no point in removing the regenerator and the heat exchangers, since even if their volume is a "dead" volume, not being swept by the pistons, their presence is fundamental for the engine to work properly. In fact, being an external combustion engine, the heat exchangers are the only thermal energy source and sink.

10.1.3 The Adiabatic Analysis

Schmidt's hypothesis that the expansion and the compression spaces are assumed to be isothermal, as a consequence of the cycle being reversible, implies that the heat is exchanged directly by these spaces with the two sources. The regenerator is also ideal. Therefore, all the heat transfer processes occurring in the real world, do not influence the Schmidt analysis.

The adiabatic analysis is a sort of improved Schmidt analysis where the expansion and compression spaces are assumed to be adiabatic. In this way, the heat enters and leaves the engine only through the heat exchangers which are distinct from the expansion and compression spaces. The adiabatic analysis is still an idealized nonlinear model of Stirling engines since it retains the assumption of ideal (*i.e.* reversible) heat exchangers and regenerator. This is still quite a heavy assumption since the heat exchangers and the regenerator are the core of Stirling machines. Therefore the adiabatic analysis can still give quite erroneous results, even if more realistic than Schmidt analysis, and predicts an overall engine efficiency not too far from the one of the Carnot cycle.

The adiabatic assumption makes it impossible to obtain a closed form solution, as it was for the Schmidt analysis and demands an iterative solving procedure to be enforced.

The main assumptions of the adiabatic analysis are:

- the thermodynamic properties of the operating fluid are constant,
- the engine consists of five spaces: the expansion space (e), the heater (h), the regenerator (r), the cooler (k), the compression space (c) (See Fig. 10.4),
- the volume variations in the expansion and compression spaces are sinusoidal and follow Eq. 10.2,
- the volumes in the heater (V_h), the regenerator (V_r), and the cooler (V_k) are constant,
- the temperatures in the heater (T_h), and the cooler (T_k) are constant and uniform,
- the temperature in the regenerator is constant and linearly varying between T_k and T_h, thus, the regenerator mean effective temperature is given by Eq. 10.4,
- the expansion and the compression spaces are adiabatic,
- the pressure is uniform within the working space ($p = p_e = p_h = p_r = p_k = p_c$), and, under the ideal gas equation, is expressed as

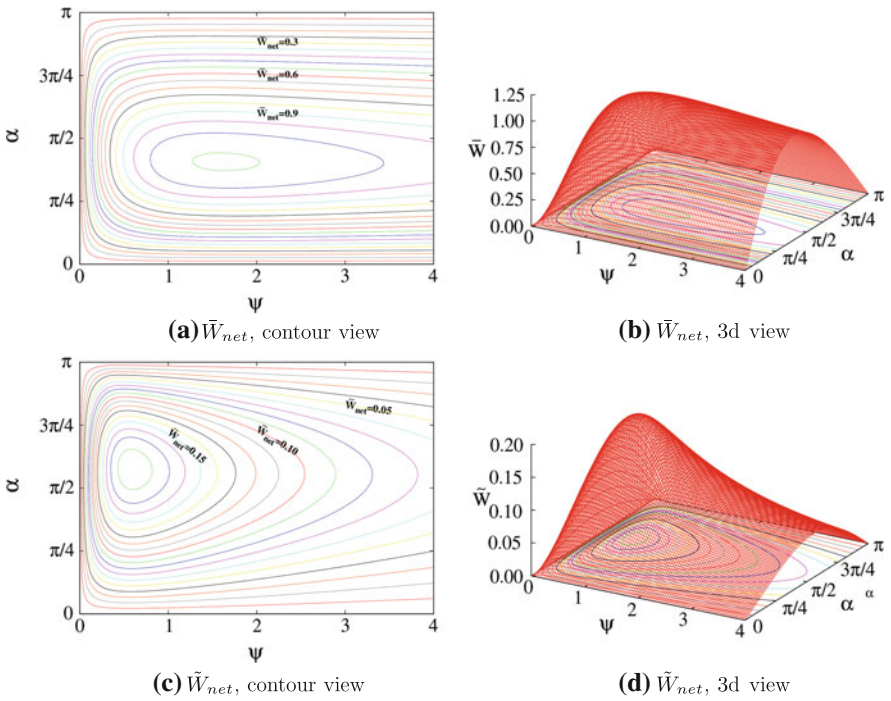

(a) $\bar{W}_{net}$, contour view **(b)** $\bar{W}_{net}$, 3d view

(c) $\tilde{W}_{net}$, contour view **(d)** $\tilde{W}_{net}$, 3d view

Fig. 10.3 Nondimensional net work output according to the Schmidt analysis as a function of ψ and α, for $\tau = \frac{1}{3}$, $x_h = \frac{1}{10}$, $x_r = \frac{1}{10}$, $x_k = \frac{1}{10}$ ($H = 0.188$)

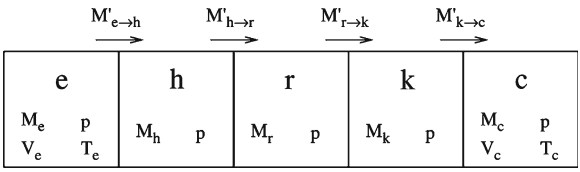

Fig. 10.4 The Stirling engine working space

$$p(\theta) = MR\left(\frac{V_c(\theta)}{T_c(\theta)} + \frac{V_k}{T_k} + \frac{V_r}{T_r} + \frac{V_h}{T_h} + \frac{V_e(\theta)}{T_e(\theta)}\right)^{-1} \tag{10.17}$$

where θ is the phase angle, M the overall mass of the operating fluid, R the thermodynamic constant, specific of the operating gas.

Solving the adiabatic analysis means to compute, for each value of the crank angle θ, the volume, the temperature, and the mass of operating fluid for each engine section, and the pressure in the working space. The amount of heat and work exchanged during the cycle are finally computed.

From the above assumptions, the adiabatic analysis depends upon ten variables:

- the volume and the temperature of the expansion and the compression spaces (V_e, V_c, T_e, T_c),
- the mass of the operating fluid in each space (M_c, M_k, M_r, M_h, M_e),
- the pressure in the working space (p).

Thus, in order to solve the adiabatic analysis, ten equations are needed, and they are:

- two volume variation equations for the expansion and the compression spaces (Eq. 10.2),
- two energy balance equations for the expansion and the compression spaces,
- five state equations, one for each space,
- one continuity equation.

For solving the energy balance equations we need to compute the mass flow rates in and out of the expansion and the compression spaces. We designate $M'_{e\to h}$ the mass flow rate from the expansion space to the heater, and $M'_{k\to c}$ the mass flow rate from the cooler to the compression space. We also define the upwind temperature at the interfaces $T_{e\to h}$, $T_{k\to c}$ which are conditional on the direction of the flow

$$T_{e\to h} = \begin{cases} T_e & \text{if } M'_{e\to h} > 0 \\ T_h & \text{if } M'_{e\to h} \le 0 \end{cases} \qquad T_{k\to c} = \begin{cases} T_k & \text{if } M'_{k\to c} > 0 \\ T_c & \text{if } M'_{k\to c} \le 0. \end{cases} \tag{10.18}$$

The state equation for a generic space and the continuity equation in differential form can be written as

$$\frac{\mathrm{d}p}{p} + \frac{\mathrm{d}V}{V} = \frac{\mathrm{d}M}{M} + \frac{\mathrm{d}T}{T} \tag{10.19}$$

$$\mathrm{d}M_e + \mathrm{d}M_h + \mathrm{d}M_r + \mathrm{d}M_k + \mathrm{d}M_c = 0 \tag{10.20}$$

respectively, where $\mathrm{d}M_e = -M'_{e\to h}$ and $\mathrm{d}M_c = M'_{k\to c}$. The energy equations for a generic space is

$$\mathrm{d}Q + c_p T_{in} M'_{in} - c_p T_{out} M'_{out} = \mathrm{d}W + c_v \mathrm{d}\,(MT) \tag{10.21}$$

which, for the expansion and the compression spaces becomes

$$-c_p T_{e\to h} M'_{e\to h} = p\,\mathrm{d}V_e + c_v \mathrm{d}\,(M_e T_e) \tag{10.22}$$

$$c_p T_{k\to c} M'_{k\to c} = p\,\mathrm{d}V_c + c_v \mathrm{d}\,(M_c T_c)\,. \tag{10.23}$$

Here, $\mathrm{d}Q$ and $\mathrm{d}W$ stand for infinitely small quantities of transferred heat and work, c_v and c_p are the specific heats of the operating fluid at constant volume and at constant pressure respectively. With a few algebraic passages Eqs. 10.22 and 10.23 can be written in the forms

$$\mathrm{d}M_e = \frac{p\,\mathrm{d}V_e + \frac{V_e}{\gamma}\mathrm{d}p}{RT_{e\to h}} \tag{10.24}$$

$$\mathrm{d}M_c = \frac{p\,\mathrm{d}V_c + \frac{V_c}{\gamma}\mathrm{d}p}{RT_{k\to c}} \tag{10.25}$$

where $\gamma = \frac{c_p}{c_v}$, $R = c_p - c_v$. By differentiating the state equation the following are derived for the heater, the regenerator, and the cooler, respectively:

$$\mathrm{d}M_h = \frac{M_h}{p}\mathrm{d}p = \frac{V_h}{RT_h}\mathrm{d}p, \qquad \mathrm{d}M_r = \frac{M_r}{p}\mathrm{d}p = \frac{V_r}{RT_r}\mathrm{d}p, \qquad \mathrm{d}M_k = \frac{M_k}{p}\mathrm{d}p = \frac{V_k}{RT_k}\mathrm{d}p \tag{10.26}$$

Substituting Eqs. 10.24–10.26 into the continuity equation, with a few algebraic passages, yields

$$\mathrm{d}p = \frac{-\gamma p\left(\frac{\mathrm{d}V_e}{T_{e\to h}} + \frac{\mathrm{d}V_c}{T_{k\to c}}\right)}{\frac{V_e}{T_{e\to h}} + \gamma\left(\frac{V_h}{T_h} + \frac{V_r}{T_r} + \frac{V_k}{T_k}\right) + \frac{V_c}{T_{k\to c}}}. \tag{10.27}$$

From the state equation, the following equations hold for the expansion and the compression spaces:

$$\mathrm{d}T_e = T_e\left(\frac{\mathrm{d}p}{p} + \frac{\mathrm{d}V_e}{V_e} - \frac{\mathrm{d}M_e}{M_e}\right), \qquad \mathrm{d}T_c = T_c\left(\frac{\mathrm{d}p}{p} + \frac{\mathrm{d}V_c}{V_c} - \frac{\mathrm{d}M_c}{M_c}\right). \tag{10.28}$$

Applying the energy equation to the heater, the cooler, and the regenerator it is possible to express the amount of heat exchanged by each section:

$$\mathrm{d}Q_h = \frac{c_v V_h \mathrm{d}p}{R} - c_p\left(T_{e\to h}M'_{e\to h} - T_h M'_{h\to r}\right) \tag{10.29}$$

$$\mathrm{d}Q_r = \frac{c_v V_r \mathrm{d}p}{R} - c_p\left(T_h M'_{h\to r} - T_k M'_{r\to k}\right) \tag{10.30}$$

$$\mathrm{d}Q_k = \frac{c_v V_k \mathrm{d}p}{R} - c_p\left(T_k M'_{r\to k} - T_{k\to c}M'_{k\to c}\right). \tag{10.31}$$

Finally, the work done is given by

$$\mathrm{d}W_e = p\,\mathrm{d}V_e, \qquad \mathrm{d}W_c = p\,\mathrm{d}V_c, \qquad \mathrm{d}W_{net} = \mathrm{d}W_e + \mathrm{d}W_c. \tag{10.32}$$

The choice of the operating fluid determines R, c_p, c_v, γ. A crank angle step size $\Delta\theta$ must be defined. The steps of the adiabatic analysis, from iteration n to iteration $n+1$, are:

- update the crank angle $\theta^{(n+1)} = \theta^{(n)} + \Delta\theta$,
- update the values of the expansion and the compression volumes (Eq. 10.2) and their derivatives $V_e^{(n+1)}$, $V_c^{(n+1)}$, $\left(\frac{\mathrm{d}V_e}{\mathrm{d}\theta}\right)^{(n+1)}$, $\left(\frac{\mathrm{d}V_c}{\mathrm{d}\theta}\right)^{(n+1)}$,

- update $T_e^{(n+1)}$, $T_c^{(n+1)}$, $W_e^{(n+1)}$, $W_c^{(n+1)}$, $Q_h^{(n+1)}$, $Q_r^{(n+1)}$, $Q_k^{(n+1)}$ by numerical integration,
- update the conditional temperatures $T_{e\to h}^{(n+1)}$, $T_{k\to c}^{(n+1)}$ (Eq. 10.18),
- update the pressure $p^{(n+1)}$ (Eq. 10.17) and the pressure derivative $\left(\frac{\mathrm{d}p}{\mathrm{d}\theta}\right)^{(n+1)}$ (Eq. 10.27),
- for each engine space, update the mass $M^{(n+1)}$ (using the ideal gas equation), the mass derivative $\left(\frac{\mathrm{d}M}{\mathrm{d}\theta}\right)^{(n+1)}$ (Eqs. 10.24–10.26), and the mass flow M' according to the following equation

$$M'_{e\to h} = -\mathrm{d}M_e, \qquad M'_{h\to r} = -\mathrm{d}M_e - \mathrm{d}M_h, \qquad M'_{r\to k} = \mathrm{d}M_c + \mathrm{d}M_k, \qquad M'_{k\to c} = \mathrm{d}M_c \tag{10.33}$$

- update the temperature derivatives $\left(\frac{\mathrm{d}T_e}{\mathrm{d}\theta}\right)^{(n+1)}$, $\left(\frac{\mathrm{d}T_c}{\mathrm{d}\theta}\right)^{(n+1)}$ (Eq. 10.28),
- update $\left(\frac{\mathrm{d}W_e}{\mathrm{d}\theta}\right)^{(n+1)}$, $\left(\frac{\mathrm{d}W_c}{\mathrm{d}\theta}\right)^{(n+1)}$, $\left(\frac{\mathrm{d}W_{net}}{\mathrm{d}\theta}\right)^{(n+1)}$, $\left(\frac{\mathrm{d}Q_h}{\mathrm{d}\theta}\right)^{(n+1)}$, $\left(\frac{\mathrm{d}Q_r}{\mathrm{d}\theta}\right)^{(n+1)}$, and $\left(\frac{\mathrm{d}Q_k}{\mathrm{d}\theta}\right)^{(n+1)}$ (Eqs. 10.29–10.32)

The adiabatic analysis, even though it is not an initial value problem, is solved as an initial value problem and the procedure is started by inputting a set of arbitrary conditions at $t = 0$ (or $\theta = 0$) and fixing a Δt (or $\Delta\theta$) step. The process above is repeated up to convergence, that is, up to when the initial transitory has been dampened out. Experience has shown that the most sensitive measure of convergence is the residual regenerator heat Q_r at the end of the cycle, which should be zero. The first order explicit Euler method [131] yields fairly accurate results for Stirling adiabatic analysis. For better accuracy, it is suggested to employ the fourth order Runge–Kutta method [132].

10.2 The Case

Typically, the optimization of any thermal engine aims at

- the maximization of the power output P_{out} of the engine,
- the maximization of the thermodynamic efficiency η of the engine.

Here, we address Stirling engines design by means of Schmidt and adiabatic analyses with these two objectives in mind. Although Schmidt and adiabatic simulations are idealized models, they are a good and cheap starting point for Stirling engines evaluation.

A Stirling engine is said to be of β type when the power piston is arranged within the same cylinder and on the same shaft as the displacer piston. Two other engine configurations are possible: α when two power pistons are arranged in two separated cylinders, and γ when a power piston and a displacer are arranged in separate cylinders. The type of the Stirling engine does not influence the Schmidt and the adiabatic analyses. Figure 10.5 shows a very simple model of a Stirling

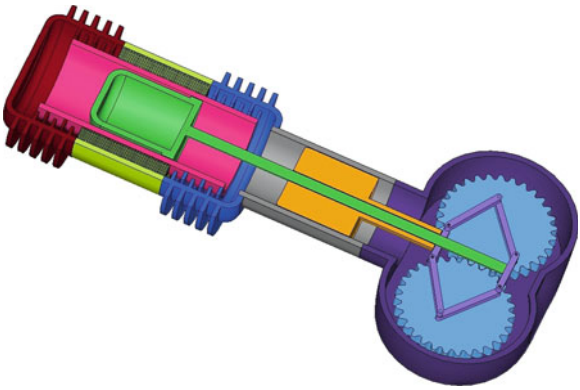

Fig. 10.5 β Stirling engine with rhombic drive

engine of β type with a rhombic drive. The rhombic drive is one of the most popular drive mechanisms for Stirling engines. In the figure are shown (top–down):

- the heater (in dark red),
- the hot cylinder wall (in pink),
- the regenerator (in yellow),
- the displacer piston (in green),
- the cooler (in blue),
- the cold cylinder wall (in grey),
- the power piston (in orange),
- the rhombic drive (in light purple),
- the drive gears (in cyan).

The idea behind the optimization experiment performed is to find the optimal configurations according to the two analytical models, and to compare the differences in the results. Of course, before running the simulations we need to define a few constraints on the engine. These constraints are necessary otherwise the optimization process would result in engines with, for instance, infinite hot temperature, volumes, and power output. The basic assumptions for the exercise are:

- Schmidt and adiabatic analysis are accepted as valid means for Stirling engine simulations and are employed in the optimization process. This is equivalent to accept the assumptions discussed in Sects. 10.1.2, 10.1.3,
- the objective of the optimization are the maximization of the engine's power output and thermodynamic efficiency

$$P_{out} = W_{net} \frac{rpm}{60}, \qquad \eta = \frac{W_{net}}{Q_{in}} \tag{10.34}$$

where rpm stands for the engine frequency in revolutions per minute, Q_{in} is the heat input to the engine in one cycle, W_{net} the work output given by the engine in

one cycle. The simulation code employed to perform the Schmidt and the adiabatic analyses was written using C++ language.

10.3 Methodological Aspects

In this section we discuss briefly and in chronological order the choices made for the setup of the optimization process. We roughly retrace the same steps seen in Chap. 8. Most of the observations made in that chapter are still valid for this application, and will not be repeated here. A schematic representation of the choices which have been made, and which will be discussed, is given in Fig. 10.6.

10.3.1 Experiments Versus Simulations

As usual there are two possible ways for collecting data: by means of experiments, or by means of simulations. In the case of a generic and introductory approach for sizing Stirling engines, there is no way to adopt the experimental approach: in a real engine, in fact, a very large number of parameters come into play, and we need some other means for collecting data quickly.

As anticipated in Sect. 10.1, we choose to address the optimization of Stirling engines using two alternative analytical methods: the Schmidt analysis and the adiabatic analysis. These are two very idealized models yielding far better results than those actually attainable in a real world application. Even if the two models are very similar, the fact that the Schmidt analysis adopts the additional simplification of isothermal expansion and compression spaces induces relevant differences in the optimization outcomes, as shown later.

10.3.2 Objectives of the Optimization

In this case, the choice of the objectives of the optimization is straightforward. In fact, the output parameters we can compute in Schmidt and adiabatic analyses are a few general informations over the cycle, like:

- maximum and minimum temperatures in the cycle, and temperature swing in the expansion and the compression spaces,
- maximum and minimum pressure, and pressure swing in the cycle,
- pressure phase angle with respect to the expansion volume variation,
- heat exchanged by the engine,
- work produced by the engine.

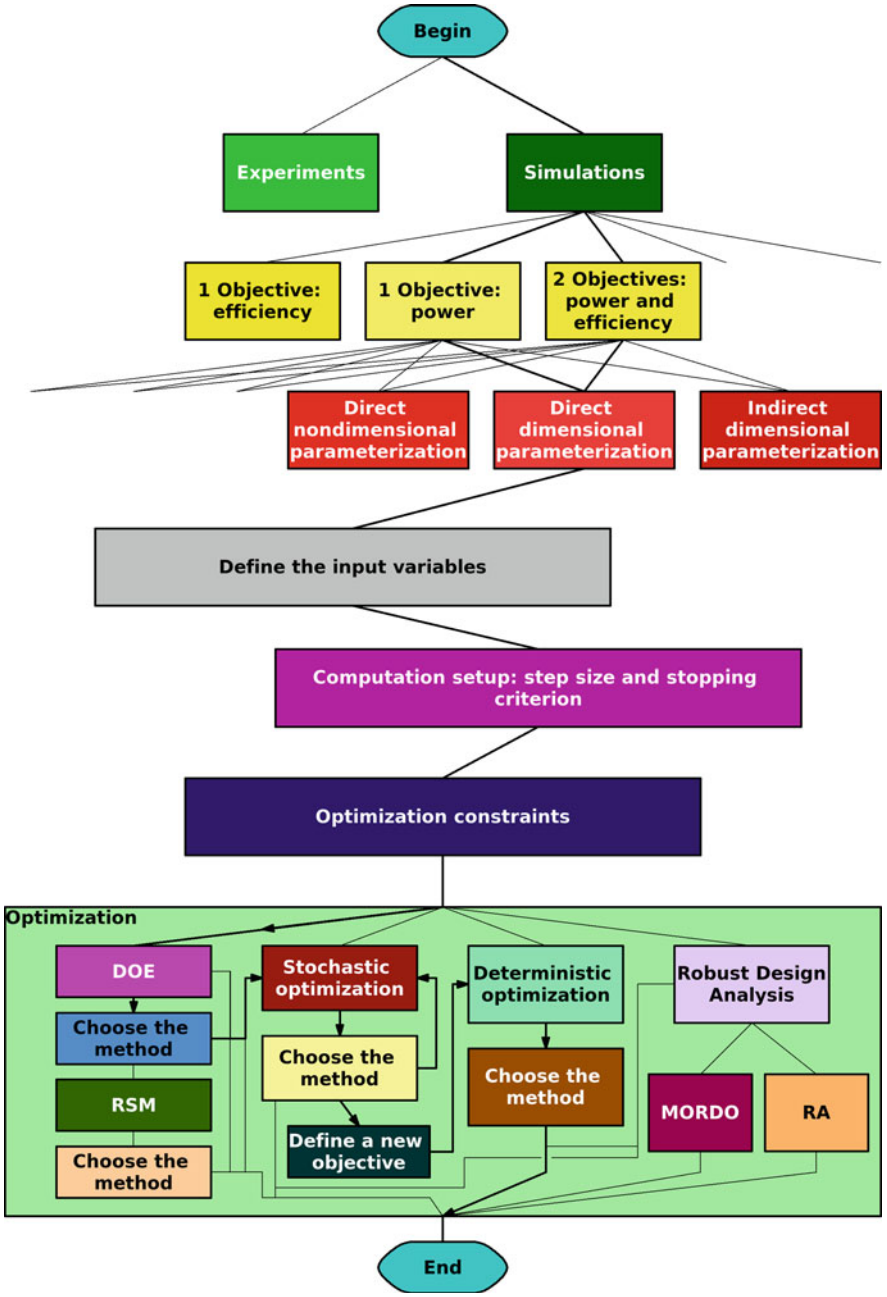

Fig. 10.6 Summary of the choices made in the setting up of the stirling engine optimization problem

Thus, the choice is quite obvious since the most interesting objectives in engines design are the work produced per cycle (or the net power output by multiplying it by the revolution speed), and the engine thermodynamic efficiency which is the ratio between the net work output and the heat input over one cycle. Schmidt and adiabatic analyses actually do not need a revolution speed to be defined. However, we define a revolution speed, which is kept constant throughout the whole optimization process, and which is just a multiplying factor allowing us to refer to the more commonly used power output, in place of the net work output per cycle as output parameter.

Since the Schmidt analysis always yields the Carnot thermodynamic efficiency, in this case we address a single objective optimization aiming at the maximization of the net power output. In the case of adiabatic analysis, instead, we address a multi-objective optimization aiming at the maximization of the net power output and the maximization of the thermodynamic efficiency of the engine.

Also the temperature and the pressure values within the engine are of interest to the designer, to avoid excessive thermal and mechanical loads on the engine components. For this reason, suitable constraints will be required over these output parameters.

However, Schmidt and adiabatic analyses just consider the thermodynamic of the engine. Other important issues in engines design are not investigated, such as, the weight of the engine components, the mechanical stresses, or the size of the heat exchangers.

10.3.3 Input Variables

The parameterizations required by the Schmidt and the adiabatic analyses are almost the same, but Schmidt's results do not depend on the gas specific heat coefficients, while adiabatic outputs do.

Fourteen parameters are included in the analysis, they are:

- the swept volumes of the expansion and compression spaces ($V_{sw,e}$ and $V_{sw,c}$),
- the dead volumes of the expansion and compression spaces ($V_{d,e}$ and $V_{d,c}$),
- the heater, regenerator, and cooler volumes (V_h, V_r, and V_k),
- the heater and cooler temperatures (T_h and T_k),
- the expansion space to compression space volume phase angle (α),
- the overall mass of operating fluid (M). This can be substituted by some other quantity defining the amount of fluid inside the engine such as, the average cycle pressure (p_m),
- the properties of the operating fluid (R and c_p),
- the revolution speed (rpm).

The parameterization is more rigid and does not allow many alternative formulations as it was in the examples discussed in Chaps. 8 and 9. These parameters can be given directly as input or can be given indirectly by defining, for instance, the type of Stirling engine, the pistons diameter and stroke, and by computing subsequently the swept volumes. Some nondimensional parameters could also be used, however,

all the alternatives are absolutely equivalent in terms of simulations and outcome of the optimization. The operating fluid which is employed in Stirling engines is commonly air, helium, or hydrogen. In general, the larger is the gas constant, the better is the engine performance, since a small change in the hot temperature is reflected in an elevated pressure driving the pistons motion. Thus, hydrogen is the best but it also brings containment problems. Second comes helium which is often employed in real engines. Air, despite its relatively low thermodynamic constant, is also often used because it is found much more easily in nature, and this makes the engine replenishment in case of pressure drop in the working space due to leakages, extremely easy.

We choose to keep the cooler temperature (T_k) and the revolution speed (rpm) constant throughout the optimization process and to consider helium as the operating fluid (thus, fixing R and c_p). The remaining parameters are adopted as input variables of the optimization.

We expect that, according to both Schmidt and adiabatic analyses, the optimal configurations which will be found when pursuing the maximization of the power output, will have approximately zero dead volumes ($V_{d,e} = V_{d,c} = V_h = V_r = V_k = 0\,\text{cm}^3$) so that the meaningful input variables will actually become five ($V_{sw,e}$, $V_{sw,c}$, α, T_h, and p_m). In fact, both the Schmidt and the adiabatic analyses consider isothermal heat exchangers and no constraint is imposed to the heat transfer rate. As a consequence, the heat exchanger volumes act as dead volumes to all intents and purposes. We also expect the hot temperature and the mean pressure to be as high as possible compatibly with the optimization constraints.

No other parameter except the step size and the stopping criterion for the adiabatic analysis needs to be defined for the setup of the simulation process.

10.3.4 Constraints

The constraints applied to the Stirling engine optimization problem go beyond the typical $x_{min} \leq x \leq x_{max}$ type.

Of course we define ranges for the input variables, in particular, we impose:

- $0\,\text{cm}^3 \leq V_{sw,e} \leq 400\,\text{cm}^3$,
- $0\,\text{cm}^3 \leq V_{sw,c} \leq 400\,\text{cm}^3$,
- $0\,\text{cm}^3 \leq V_{d,e} \leq 100\,\text{cm}^3$,
- $0\,\text{cm}^3 \leq V_{d,c} \leq 100\,\text{cm}^3$,
- $0\,\text{cm}^3 \leq V_h \leq 100\,\text{cm}^3$,
- $0\,\text{cm}^3 \leq V_r \leq 100\,\text{cm}^3$,
- $0\,\text{cm}^3 \leq V_k \leq 100\,\text{cm}^3$,
- $350\,\text{K} \leq T_h \leq 900\,\text{K}$,
- $T_k = 300\,\text{K}$,
- $-\pi \leq \alpha \leq \pi$,
- $1\,\text{bar} \leq p_m \leq 49\,\text{bar}$,

- $R = 2077 \frac{\text{J}}{\text{kg, K}}$,
- $c_p = 5193 \frac{\text{J}}{\text{kg, K}}$,
- $rpm = 600\,\text{rpm}$.

Additional constraints are given in order to limit the engine's size, the stress due to the pressure, and the engine minimum power output:

- $V_{sw,e} + V_{d,e} + V_h + V_r + V_c + V_{d,c} + V_{sw,c} \leq 500\,\text{cm}^3$,
- $p_{max} \leq 50\,\text{bar}$,
- $P_{net} \geq 300\,\text{W}$.

The last constraint was added to prevent the multi-objective optimization to move towards zero power output configurations, which are likely to happen pursuing the objective of maximum thermodynamic efficiency.

The ranges of the input variables are restricted as the optimization process goes on.

10.3.5 The Chosen Optimization Process

A similar optimization process is applied twice, using the Schmidt analysis first, and then using the adiabatic analysis. The simulation process is a cheap analytical computation which requires a fraction of a second to be completed on a personal computer. For this reason, this optimization exercise is also used for comparing different optimization methods.

We start from considering the Schmidt analysis for the ten input variables problem. At first a Sobol DOE with 2048 feasible designs is performed. The range of the input variables is then restricted around the optimum solution found, and a 1P1-ES stochastic optimization with 1024 designs is applied. The range of the input variables is restricted once again around the optimum configuration found, and a Nelder and Mead simplex deterministic algorithm is applied in the end.

As for the adiabatic analysis for the ten input variables problem, A Sobol DOE with 2048 feasible designs is performed first. Then the range of the input variables is restricted, and a MOGA with 4096 designs (32 individuals $\times$ 128 generations) is applied. The MOGA is followed by two 1P1-ES with 1024 designs each: the first aiming at the maximization of the power output, the second aiming at the maximization of the engine's thermodynamic efficiency. The two 1P1-ES are followed by two Nelder and Mead simplex optimizations having the same objectives as the evolutionary optimizations.

Thus, the procedures followed for the Schmidt and the adiabatic analyses are much the same. The differences are that:

- no MOGA is performed using Schmidt analysis, since for the Schmidt case the thermodynamic efficiency objective loses its significance,
- the evolutionary and the simplex steps are performed twice, once for each optimization objective, in the adiabatic analysis.

As expected, the results of the optimization tend to lead to configurations with zero dead volume, maximum heater temperature, and maximum total volume, where the total volume is

$$V_{tot} = V_{sw,e} + V_{d,e} + V_h + V_r + V_k + V_{d,c} + V_{sw,c}. \tag{10.35}$$

For this reason, in the second part of the optimization process, the heater temperature is fixed to 900 K, the dead volumes to zero, and the compression swept space to $V_{sw,c} = 500\,\text{cm}^3 - V_{sw,e}$. In this way, we define an optimization problem whose three variables are: $V_{sw,e}$, α, p_{mean}. Over the new optimization problem the same optimization process adopted for the ten input variables case is applied, thus involving: a Sobol DOE, a MOGA optimization, a 1P1-ES optimization, and a Nelder and Mead simplex optimization. Each optimization algorithm was initialized from the best configurations found in the previous step of the process. Actually, the zero dead volume condition is approached only when the net power output objective is addressed. When the thermodynamic efficiency is addressed, the optimal solutions present large dead volumes and very poor performance in terms of power output. The reason for this, is that the thermodynamic efficiency reduction in the adiabatic analysis is due to the non-isothermal behaviour of the expansion and the compression spaces. Temperature variations in the expansion and the compression spaces are mainly due to the pressure variation in the working space caused by the pistons motion. For this reason, the thermodynamic efficiency is high when

- the swept volumes are low, since a low swept volume means also a low pressure variation in the working space over the cycle,
- the dead volumes are large, since the dead volumes act as a buffer volume containing the pressure and temperature variations in the working space.

These two conditions heavily and negatively affect the engine performance in terms of power output. Since the simulations require a very short computing time to be completed, in the last part of the optimization process, several optimization techniques were compared starting from scratch, using the same initial design point or population, and the same design space. Single objectives techniques were compared over the Schmidt analysis, and multi-objective techniques were compared over the adiabatic analysis. The comparison also included a few DOE+RSM techniques coupled to metamodel-assisted optimization processes.

A summary of the elements involved in the first two parts of the optimization process is given in Fig. 10.7.

10.4 Results

Let us consider the ten variables Schmidt optimization problem. The results of the Sobol DOE, the 1P1-ES, and the simplex optimizations are summarized in Table 10.1. The whole optimization process is carried out by using the optimization dedicated

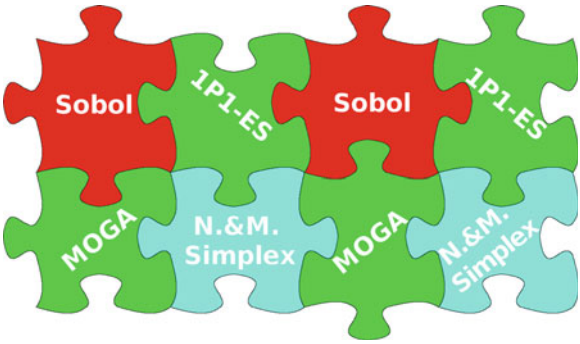

Fig. 10.7 Elements involved in the Stirling engine optimization problem

Table 10.1 Ten input variables optimization: Schmidt analysis results

Input Variable	*Sobol* DOE (2048 designs)			1P1-ES (1024 designs)			Simplex (1083 designs)		
or Output	Range		Best	Range		Best	Range		Best
Parameter	Low	High	P_{net}	Low	High	P_{net}	Low	High	P_{net}
α [deg]	−180	180	123.53	10	170	110.05	80	150	111.91
T_h [K]	350	900	839.51	400	900	888.39	600	900	899.96
$V_{sw,e}$ [cm^3]	0	400	288.62	10	350	319.86	50	350	329.92
$V_{sw,c}$ [cm^3]	0	400	114.40	10	350	175.04	50	350	169.41
$V_{d,e}$ [cm^3]	0	100	22.60	0	100	1.73	0	50	0.01
$V_{d,c}$ [cm^3]	0	100	8.58	0	100	0.00	0	50	0.23
V_h [cm^3]	0	100	24.60	0	100	2.66	0	50	0.11
V_r [cm^3]	0	100	21.35	0	100	0.55	0	50	0.30
V_k [cm^3]	0	100	5.60	0	100	0.00	0	50	0.00
p_m [bar]	1	49	29.26	4	46	24.94	15	40	25.58
M [g]	–	–	0.671	–	–	0.460	–	–	0.466
p_{max} [bar]	–	–	41.69	–	–	49.70	–	–	50.00
V_{tot} [cm^3]	–	–	485.75	–	–	499.85	–	–	499.99
P_{net} [kW]	–	–	**2.756**	–	–	**5.285**	–	–	**5.474**
η [%]	–	–	64.26	–	–	66.23	–	–	66.67

software *mode*FRONTIER. At each step, the design space size is shrinked around the best configuration found in the previous step. As expected, the optimization is clearly moving towards an optimum configuration with zero dead volumes, heater temperature of 900 K, total volume of 500 cm^3, and maximum pressure in the cycle of 50 bar. Despite 2048 configurations were evaluated in the Sobol DOE, the best result found by the process is still far from the optimality condition. In fact, the number of input variables is rather large, and a deep investigation of the design space is not attained even with such a number of simulations.

A stochastic optimization is more precise in finding optimum solutions than pseudo-random searches. In fact, passing from the Sobol sampling to the 1P1-ES

the performance of the better configuration in terms of maximum net power output is almost double. Deterministic optimization is even more precise than stochastic optimization, and the performance of the better configuration is further improved after the simplex optimization. Thus, the procedure starts from a quasi-random exploration of the design space and moves on, step by step, towards an accurate refinement of the solution.

The choice of any optimization process is always a trade-off between how much importance is given to the design space exploration and to the solution refinement, that is, between robustness and velocity. By robustness the capability of avoiding local optima and explore the whole design space is meant.

The same procedure is followed for the ten variables adiabatic optimization problem, whose results are summarized in Table 10.2. Since in the adiabatic analysis we address two objectives, we also apply multi-objective optimization algorithms. The results in terms of maximization of the net power output (right hand of the Pareto frontiers in Fig. 10.8) go in the same direction of those found for the Schmidt analysis (zero dead volume, maximum heater temperature, maximum total volume, maximum average pressure compatibly with the maximum pressure constraint). As for the maximum thermodynamic efficiency objective, as already noted, it must be considered that the source of inefficiency in the adiabatic analysis is due to the non-isothermal behaviour of the expansion and the compression spaces. Thus, the least is the temperature variation in those spaces, the better is the efficiency. However, the least is the temperature variation, the worse is the net power output due to the small working space compression needed for causing small temperature variations. An additional constraint on the minimum net power required from the engine is given in order to avoid degenerate solutions. Despite this constraint, it is clear from Table 10.2 that the optimum solutions in terms of thermodynamic efficiency have small compression and expansion space swept volume, elevated dead volume, high mean pressure, low pressure and temperatures swing in the working space over the cycle. In other words, if it was not for the constraint given on the net power output, the optimum configuration would have moved towards an engine which stands still and, obviously, gives no power output.

In the second part of the optimization procedure

- the dead volumes are fixed to zero,
- the total volume is fixed to 500 cm^3,
- the heater temperature is fixed to 900 K,

that is, the number of input variables is reduced to three. Actually, the dead volumes are fixed to 1 mm^3 each, since zero dead volumes causes the adiabatic analysis to diverge. The design space is further reduced at each step in a neighbourhood of the optimum solutions previously found. Table 10.3 shows the results of the three input variables Schmidt optimization; Table 10.4 shows the results of the three input variables adiabatic optimization.

The adiabatic optimization has a larger design space since it must follow the tendencies of the two objectives of the optimization. Now that there is no dead volume to play with, when pursuing the maximization of the thermodynamic efficiency, the

Table 10.2 Ten input variables optimization: adiabatic analysis results

Input variable or Output parameter	*Sobol* DOE (2048 designs)				MOGA-II (4096 designs)				1P1-ES (2 × 1024 designs)				Simplex (953 + 437 designs)			
	Range		Best	Best	Range		Best	Best	Range		Best	Best	Range		Best	Best
	Low	High	P_{net}	η	Low	High	P_{net}	η	Low	High	P_{net}	η	Low	High	P_{net}	η
α [deg]	−180	180	123.5	112.1	10	170	134.5	169.8	10	170	142.5	166.4	80	170	140.7	169.0
T_h [K]	350	900	839.5	884.3	400	900	900.0	900.0	400	900	900.0	899.8	600	900	882.1	900.0
$V_{sw,e}$[cm^3]	0	400	288.6	91.4	10	350	286.1	231.8	10	350	302.8	164.2	50	350	304.4	180.1
$V_{sw,c}$ [cm^3]	0	400	114.4	34.7	10	350	108.0	81.1	10	350	156.4	60.2	50	350	168.6	68.2
$V_{d,e}$ [cm^3]	0	100	22.6	15.3	0	100	20.4	23.9	0	100	21.5	22.7	0	100	18.2	20.9
$V_{d,c}$ [cm^3]	0	100	8.6	77.6	0	100	31.8	44.9	0	100	0.1	75.5	0	100	1.8	76.5
V_h [cm^3]	0	100	24.6	37.5	0	100	32.9	0.0	0	100	9.2	38.4	0	100	3.4	42.2
V_r [cm^3]	0	100	21.4	50.2	0	100	4.5	14.3	0	100	9.6	63.2	0	100	0.3	59.6
V_k [cm^3]	0	100	5.6	49.0	0	100	4.5	100.0	0	100	0.1	51.5	0	100	3.2	50.3
p_m [bar]	1	49	29.3	43.7	4	46	32.7	38.8	4	46	31.5	45.5	19	46	29.9	45.6
$T_{e,max}$ [K]	–	–	864.0	892.2	–	–	921.7	903.5	–	–	942.3	903.8	–	–	929.3	905.1
$T_{e,min}$ [K]	–	–	576.6	816.5	–	–	676.7	876.0	–	–	632.0	875.3	–	–	596.5	876.8
$T_{c,max}$ [K]	–	–	428.9	324.6	–	–	394.4	308.0	–	–	417.2	307.9	–	–	431.9	307.5
$T_{c,min}$ [K]	–	–	281.7	295.4	–	–	287.9	298.6	–	–	276.5	298.2	–	–	274.1	298.0
M [g]	–	–	0.671	1.433	–	–	0.803	1.493	–	–	0.686	1.750	–	–	0.662	1.788
p_{max} [bar]	–	–	48.0	49.5	–	–	49.0	40.4	–	–	49.9	47.5	–	–	50.0	47.4
V_{tot} [cm^3]	–	–	485.8	355.7	–	–	488.2	496.0	–	–	499.6	475.8	–	–	500.0	497.7
P_{net} [kW]	–	–	**2.613**	**0.397**	–	–	**2.865**	**0.355**	–	–	**3.866**	**0.300**	–	–	**3.908**	**0.301**
η [%]	–	–	**50.18**	**63.86**	–	–	**57.05**	**66.33**	–	–	**54.47**	**66.56**	–	–	**51.99**	**66.67**

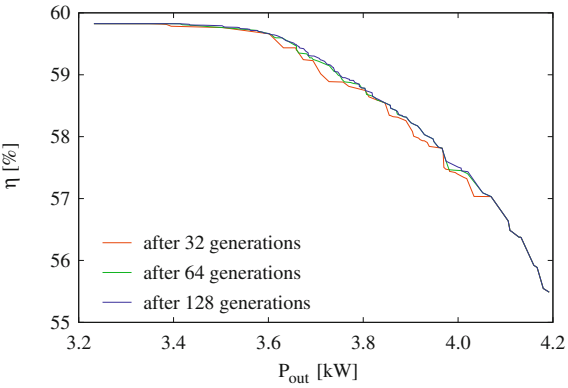

Fig. 10.8 Evolution of the Pareto frontier for the Stirling engine adiabatic analysis MOGA optimization

results of the optimization find a different strategy for limiting the temperature swing in the expansion and the compression spaces. This strategy tends to promote high values of α, as demonstrated by the results in Table 10.4. In fact, a high value of α means that the volume variations in the expansion and the compression spaces are almost in counterphase so that when the expansion space is large, the compression space is small and viceversa. Overall, the size of the working space $(V_e(\theta) + V_c(\theta))$ is not undergoing large variations over the cycle. As a result the ratios $\frac{p_{max}}{p_m}$ and $\frac{T_{max}}{T_{min}}$ are reduced. Simplex algorithm brought no improvement at all for the adiabatic analysis optimization, and a very small improvement for the Schmidt analysis optimization. This could mean that the 1P1-ES algorithm had already reached the optimum solution, at least locally.

The results of the comparison between different single objective algorithms over the three variables Schmidt optimization are shown if Fig. 10.9 and Table 10.5. All the algorithms were started from the same initial point.

BFGS and Levenberg–Marquardt algorithms fail to converge to the optimum solution. The reason for this failure is the same already discussed in the context of Example 4.1. In fact, the initial point of the optimization is near to the border of the feasible region, since the value of its maximum pressure over the cycle is almost 50 bar. However, the gradient pushes the algorithm to increase the mean pressure in the cycle because the mean pressure is proportional to the net power output. In this way, the maximum pressure constraint is violated, the objective function is penalized, and the gradient estimation is incorrect. As a result, the algorithms get stuck almost immediately. This shows that BFGS and Levenberg-Marquardt algorithms, even being very effective, only work properly in unconstrained optimization; their application to constrained optimization problems is likely to fail as soon as a constraint is violated during the optimization process. The remaining algorithms have comparable efficiency. 1P1-ES shows a slower convergence rate, while the DES is not only faster than 1P1-ES, as expected, but, surprisingly, is also almost as fast as the simplex and the NLPQLP algorithms. NLPQLP encounters problems in the

Table 10.3 Three input variables optimization: Schmidt analysis results

Input variable or Output parameter	*Sobol* DOE (2048 designs) Range Low	High	Best P_{net}	1P1-ES (1024 designs) Range Low	High	Best P_{net}	Simplex (154 designs) Range Low	High	Best P_{net}
α [deg]	90	130	115.06	100	130	112.50	100	130	113.48
$V_{sw,e}$ [cm^3]	150	400	347.88	200	400	340.97	250	400	342.84
$V_{sw,c}$ [cm^3]	100	350	152.12	100	300	159.03	100	250	157.16
p_m [bar]	21	29	26.81	23	29	26.07	24	29	26.39
M [g]	–	–	0.482	–	–	0.468	–	–	0.475
p_{max} [bar]	–	–	49.67	–	–	50.00	–	–	50.00
P_{net} [kW]	–	–	**5.469**	–	–	**5.512**	–	–	**5.513**
η [%]	–	–	66.67	–	–	66.67	–	–	66.67

Table 10.4 Three input variables optimization: adiabatic analysis results

Input variable or Output parameter	*Sobol* DOE (2048 designs)				MOGA-II (4096 designs)				1P1-ES (2 × 1024 designs)				Simplex (165 + 49 designs)			
	Range		Best	Best	Range		Best	Best	Range		Best	Best	Range		Best	Best
	Low	High	P_{net}	η	Low	High	P_{net}	η	Low	High	P_{net}	η	Low	High	P_{net}	η
α [deg]	110	160	140.7	159.7	110	160	151.0	160.0	110	160	146.2	160.0	110	160	146.2	160.0
$V_{sw,e}$ [cm^3]	250	400	310.4	372.2	250	400	333.6	365.9	250	400	329.5	365.9	250	400	329.5	365.9
$V_{sw,c}$ [cm^3]	100	250	189.6	127.8	100	250	166.4	134.1	100	250	170.5	134.1	100	250	170.5	134.1
p_m [bar]	20	40	27.1	30.9	20	40	32.2	35.6	20	40	30.2	23.2	20	40	30.2	23.2
$T_{e,max}$ [K]	–	–	1009.2	927.2	–	–	995.0	942.6	–	–	998.9	942.5	–	–	998.9	942.5
$T_{e,min}$ [K]	–	–	569.0	725.5	–	–	650.4	730.3	–	–	616.9	730.3	–	–	616.9	730.3
$T_{c,max}$ [K]	–	–	458.1	368.9	–	–	408.1	367.0	–	–	427.9	367.0	–	–	427.9	367.0
$T_{c,min}$ [K]	–	–	204.0	289.5	–	–	129.0	276.6	–	–	230.3	276.6	–	–	230.3	276.6
M [g]	–	–	0.574	0.615	–	–	0.681	0.719	–	–	0.634	0.470	–	–	0.634	0.470
p_{max} [bar]	–	–	49.9	42.0	–	–	49.9	47.5	–	–	50.0	31.1	–	–	50.0	31.1
P_{net} [kW]	–	–	**4.154**	**2.718**	–	–	**4.192**	**3.232**	–	–	**4.274**	**2.112**	–	–	**4.274**	**2.112**
η [%]	–	–	**50.14**	**59.64**	–	–	**55.49**	**59.82**	–	–	**53.42**	**59.82**	–	–	**53.42**	**59.82**

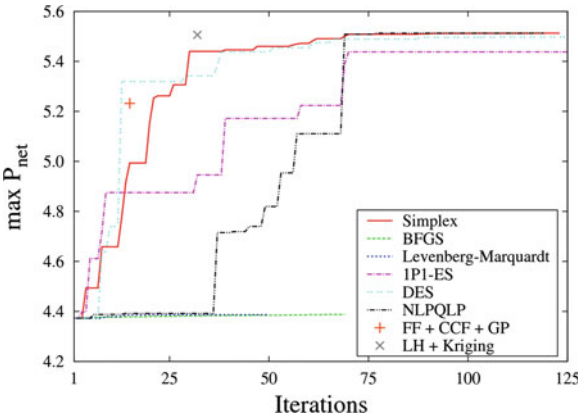

Fig. 10.9 Convergence speed of different methods over the three variables Stirling engine optimization problem through Schmidt analysis

first iterations and still yields no improvement after 35 iterations, but later it quickly makes up for the lost time and at iteration 70 is leading over all other algorithms.

Trying to generalize the above observations, let us suppose the simulations we are running are computationally intensive and each iteration requires 6 h of CPU time to complete. The deterministic optimization algorithms, unless they were failing, would have required between two and three weeks time (56–84 simulations) to reach a reasonably good approximation of the optimum configuration, and at least one month (120 simulations) to meet the stopping criterion and terminate. If we want to speed up the optimization process we could barter accuracy for speed using a DOE+RSM approach. We have tried two different DOE+RSM approaches:

- a 2-levels full factorial DOE (8 designs) plus a 3 levels central composite faced DOE (7 designs) coupled to a Gaussian process response surface,
- a uniformly distributed latin hypercube using 32 designs coupled to a Kriging response surface.

According to our hypothesis the first would have required less than 4 days of CPU time (let us say, a long week end, from friday late afternoon to tuesday morning), and the second 8 days. An optimization process could then be applied to the metamodel running in a fraction of a second. Fortunately the Schmidt analysis requires less than 0.1 sec to complete and we do not have to worry about CPU time, actually. However, the two DOE+RSM processes discussed above gave amazingly accurate results considering the small number of simuations they required (see Fig. 10.9 and Table 10.5).

It is true that using metamodels means to accept some potential degree of inaccuracy in predictions, however, it can also save a lot of time sometimes. The results of the comparison between different multi-objective algorithms over the three variables adiabatic optimization are shown in Table 10.6 and Fig. 10.10.

Table 10.5 Best configurations found by different methods over the three variables Stirling engine optimization problem through Schmidt analysis

Input	Range		Initial	N. & M.	BFGS	Leven.	1P1-ES	DES	NLPQLP	CCF+GP		LH+Kriging	
Output	Low	High	Point	Simplex		Marq.				esteem	true	esteem	true
α [deg]	90	130	120.00	113.37	119.94	119.98	106.98	109.67	113.36	118.84		112.57	
$V_{sw,e}$ [cm^3]	200	400	250.00	341.30	250.01	250.0	340.15	341.81	342.44	305.70		341.64	
$V_{sw,c}$ [cm^3]	100	300	250.00	158.70	249.99	250.0	159.85	158.19	157.56	194.30		158.36	
p_m [bar]	20	30	22.50	26.31	22.56	22.57	24.58	25.34	26.35	25.85		26.08	
M [g]	–	–	0.451	0.474	0.452	0.453	0.427	0.446	0.474	0.466	0.503	0.467	0.468
p_{max} [bar]	–	–	49.84	50.00	49.97	49.99	49.97	50.00	50.00	50.00	49.79	50.00	49.94
P_{net} [kW]	–	–	**4.373**	**5.512**	**4.387**	**4.387**	**5.466**	**5.498**	**5.513**	**5.204**	**5.232**	**5.507**	**5.506**
η [%]	–	–	66.67	66.67	66.67	66.67	66.67	66.67	66.67	66.67	66.67	66.67	66.67
Cost [iter]	–	–	–	123	69	50	150	150	119	15		32	

Table 10.6 Pareto extremity configurations found by different methods over the three variables Stirling engine optimization problem through adiabatic analysis

Input	Range		MOGA		MOSA		NSGA		MMES		MOGT	
Output	Low	High	max P_{net}	max η	max P_{net}	max η	max P_{net}	max η	max P_{net}	max η	max P_{net}	max η
α [deg]	120	160	144.52	159.66	147.62	159.87	145.75	160.00	145.38	159.99	126.65	148.20
$V_{sw,e}$ [cm^3]	200	400	316.70	361.55	334.09	368.54	336.09	365.65	337.98	358.15	340.58	379.82
$V_{sw,c}$ [cm^3]	100	300	183.30	138.45	165.91	131.46	163.91	134.35	162.02	141.85	159.42	120.18
p_m [bar]	20	40	28.76	35.89	30.87	24.46	30.31	36.00	30.18	32.10	22.50	22.50
$T_{e,max}$ [K]	–	–	961.42	920.51	945.54	915.80	943.74	917.52	942.18	923.05	942.26	915.91
$T_{e,min}$ [K]	–	–	596.27	727.53	629.40	728.67	618.82	730.30	617.48	729.08	499.68	631.63
$T_{c,max}$ [K]	–	–	440.01	368.47	420.49	367.64	427.05	367.03	427.93	367.80	512.35	415.86
$T_{c,min}$ [K]	–	–	270.78	291.21	278.55	293.02	278.75	292.39	279.30	290.29	272.09	290.82
M [g]	–	–	0.612	0.732	0.647	0.491	0.630	0.728	0.625	0.660	0.434	0.428
p_{max} [bar]	–	–	49.95	48.04	49.84	32.86	49.99	48.09	49.92	42.79	48.86	37.34
P_{net} [kW]	–	–	**4.226**	**3.387**	**4.249**	**2.193**	**4.261**	**3.275**	**4.243**	**3.050**	**3.406**	**2.493**
η [%]	–	–	**52.06**	**59.67**	**54.20**	**59.77**	**53.53**	**59.83**	**53.45**	**59.73**	**44.56**	**54.64**

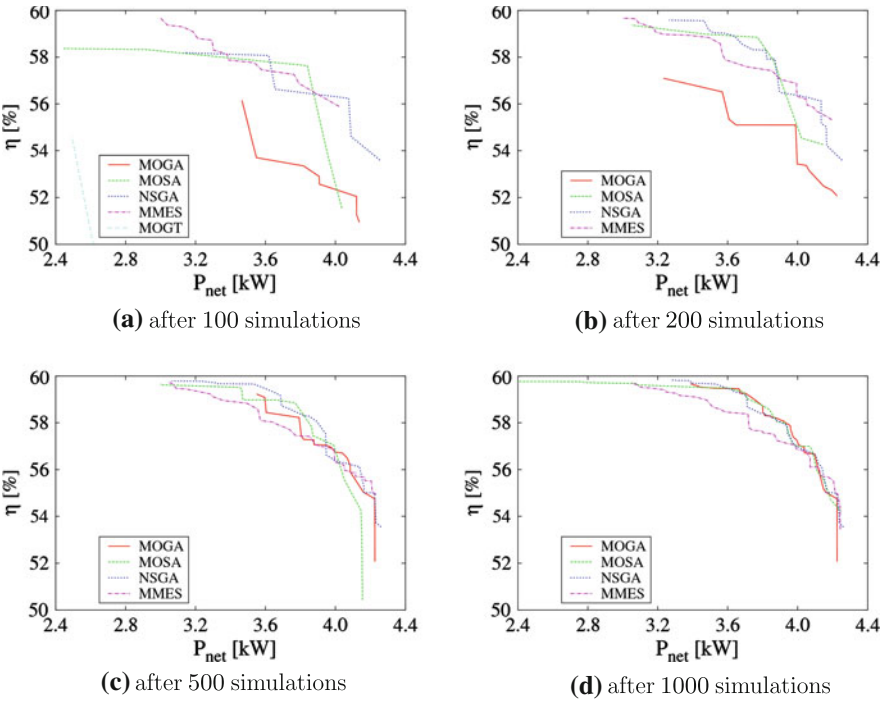

(a) after 100 simulations

(b) after 200 simulations

(c) after 500 simulations

(d) after 1000 simulations

Fig. 10.10 Pareto frontier evolution for different methods over the three variables Stirling engine optimization problem through adiabatic analysis

MOGA, MOSA, and NSGA were started from the same population of 12 individual obtained with a Sobol DOE and ran for 84 generations so that the number of simulations was reaching 1, 000 at the end of the optimization. Note that a large part of the design space defined by the ranges in Table 10.6 is considered "unfeasible" since it causes the results of the adiabatic analysis to break the maximum pressure constraint. For instance, out of the 12 individuals of the initial population 10 were unfeasible. The MMES was started from a population of 4 individuals (2 feasible and 2 unfeasible) taken from the MOGA initial population, and ran for 50 generations using an adaptive (4, 20)-ES scheme with maximum individual life span of 5 iterations. MOGT was started from a feasible individual of the MOGA initial population. The remaining parameters for the setup of the optimization were as in Example 5.1, except for the MOSA which was started from a temperature of 0.2 and had $\frac{4}{10}$ fraction of hot iterations.

Due to the strong limitations caused by the maximum pressure constraint, MOGT failed to converge and stopped after 62 simulations, 59 of which were unfeasible. The incidence of unfeasible samples is limited to 18 % in MOGA, 22 % in MOSA, 25 % in NSGA, and 9.5 % in MMES. Apart from MOGT, the other algorithms show a rather good convergence towards the Pareto frontier (see Fig. 10.10), MMES being

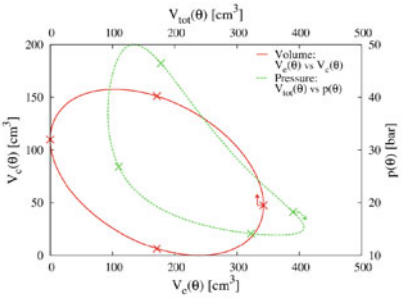

(a) NLPQLP optimum configuration after Tab. 10.5: phase plane volumes and pressure plots

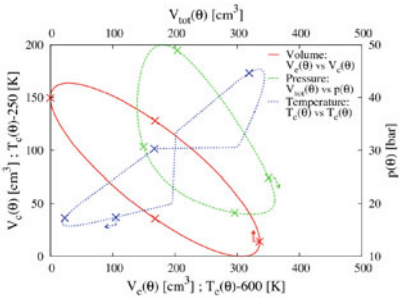

(b) NSGA max P_{net} optimum configuration after Tab. 10.6: phase plane volumes, pressure, and temperatures plots

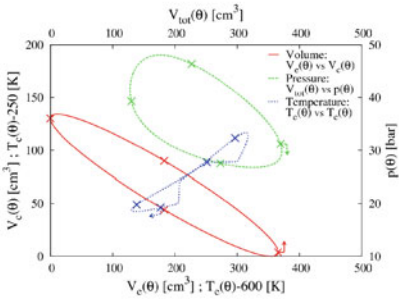

(c) NSGA max η optimum configuration after Tab. 10.6: phase plane volumes, pressure, and temperatures plots

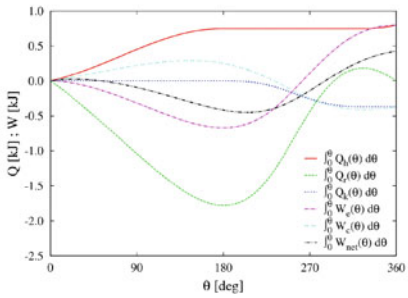

(d) NSGA max P_{net} optimum configuration after Tab. 10.6: work and heat quantities exchanged over one cycle

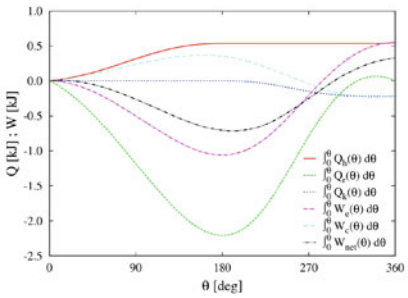

(e) NSGA max η optimum configuration after Tab. 10.6: work and heat quantities exchanged over one cycle

Fig. 10.11 Thermodynamic cycle details for some optimum configurations after Tables 10.5 and 10.6. The × signs in the phase plane plots are placed every $\Delta\theta = 90^{o}$ crank angle, the arrow individuates the $\theta = 0^{o}$ locations and the direction in which the path is travelled

slightly less efficient than the other methods towards the end of the process (after iteration 500), and MOGA being less efficient at the beginning of the process (before iteration 200). The final Pareto population is made of 43 individuals for MOGA, 27 individuals for MOSA, 66 individuals for NSGA, and 49 individuals for MMES.

Figure 10.11 shows some information about the thermodynamic cycle of the optimum configuration reported in Table 10.5 found by the NLPQLP optimization algorithm through Schmidt analysis, and by the optimum configurations reported in Table 10.6 found by the NSGA optimization algorithm through adiabatic analysis.

The irregular shape of the temperature phase plot in Fig. 10.11b, c is due to the fact that the expansion and the compression space dead volumes are zero. The process is as follows: we consider the expansion space, as initially containing a certain amount of fluid at a certain temperature; as the space is reduced to zero the fluid is ejected from the space completely; fresh fluid enters the space when the piston recedes. The incoming fluid, however, has temperature T_h due to the conditional temperature in Eq. 10.18, no matter what the temperature of the operating fluid in the space was before. This originates the discontinuities in the fluid temperature observed in the expansion space, and in the compression space. The effect would have been avoided if the dead volumes were present, since dead volumes act as buffers, hence smoothing out the sudden temperature change in the spaces due to the incoming operating fluid from the heat exchangers.

Note that, if the adiabatic simulation has reached convergence the energy balance equations are fulfilled: at the end of the cycle we have $\oint Q_r = 0$, $\oint Q_h = \oint W_e$, and $\oint Q_k = \oint W_c$ (see Fig. 10.11d, e).

10.5 Conclusions

The optimization of Stirling engines has been addressed by using the Schmidt and the adiabatic analyses. The optimization process was performed for each type of analysis. The process was quite standard and involved a Sobol DOE, a MOGA, a 1P1-ES, and a simplex optimization. After the optimization process was completed, it was noted that some input variables were moving towards one extremity of their range. When such a behaviour is found, it is clear that the input variables would move even furhter if they were not constrained by their ranges. Under these circumstances, two possible choices are suggested:

- if possible, move the ranges to comply with the tendencies of the input variables, this could lead to better performing solutions,
- if not possible, change the input variables to constants and proceed with the optimization process.

In our case, since negative volumes have no physical meaning, and a higher heater temperature would have damaged the engine, we can not move the variables ranges and we choose the second possibility. In this way, we help the optimizer to mantain the optimum values for some of the variables. In fact, due to the randomness which is present in stochastic optimization the optimizer found difficulties in keeping the values of these variables anchored to the extremity, thus wasting time running suboptimal simulations. Moreover we can now proceed with an easier optimization task which will run faster since it involves a lower number of input variables. After

the number of input variables was decreased, the same optimization process was repeated for the "reduced" problem. This strategy was successful in reaching an optimum solution and to further improve it. This latter task was achieved by both reducing the number of variables, and by progressively moving from an initial exploration of the design space by means of a Sobol DOE or a MOGA optimization, to a refinement of the solution through a Nelder and Mead simplex optimization.

The results given by the two analyses in terms of optimum engines are quite different from each other, not only for the fact that the Schmidt optimization is single objective and the adiabatic optimization is two-objectives. For instance, let us consider the optimum configurations in terms of maximization of the net power output from Tables 10.3 and 10.4

- for the Schmidt analysis we have:
  $\alpha = 113.5\,^{\circ}$, $V_{sw,e} = 342.8\,\text{cm}^3$, $V_{sw,c} = 157.2\,\text{cm}^3$, $p_m = 26.4\,\text{bar}$, $P_{net} = 5.513\,\text{kW}$,
- for the adiabatic analysis we have:
  $\alpha = 146.2\,^{\circ}$, $V_{sw,e} = 329.5\,\text{cm}^3$, $V_{sw,c} = 170.5\,\text{cm}^3$, $p_m = 30.2\,\text{bar}$, $P_{net} = 4.274\,\text{kW}$.

The main difference in the two configurations is in the larger α value which is attained in the adiabatic analysis. This causes the compression rate $\frac{p_{max}}{p_m}$ to be reduced over the cycle, which allows higher mean pressures to be applied to the engine without breaking the maximum pressure constraint. It also causes the ellipse in the volumes phase plot in Fig. 10.11 to be more elongated and tilted towards the left side of the plot.

From the point of view of optimization it is interesting the comparison between different methods, as discussed in the previous section and summarized in Tables 10.5 and 10.6, and in Figs. 10.9, 10.10, and 10.11.

It could be argued that too many constraints were applied to the optimization problem. For instance, the $P_{net} \geq 0.3\,\text{kW}$ was somewhat limiting the maximum efficiency solutions which were found. However, as it was already reminded before, this constraint was due to the fact that it was clear that the engine would have moved towards a degenerate solution. The $\alpha \leq 160\,^{\circ}$ constraint applied in the end was limiting even more the action of the optimization algorithms in terms of maximization of the thermodynamic efficiency. In fact, all the maximum efficiency optimum solutions in Tables 10.4 and 10.6 have the value of α at $160\,^{\circ}$ or very close to $160\,^{\circ}$. This indicates that the optimizer would have gone further if it could, tilting and elongating even more the volume phase plot in Fig. 10.11, increasing p_m towards 50 bar, and reducing the net power output up to when the $P_{net} \geq 0.3\,\text{kW}$ constraint was met.

It would be interesting to investigate the Stirling engine optimization problem using more advanced and realistic simulation models. The results found in this exercise for α are quite similar to the values which are used in real engines, while the swept volumes ratio $\frac{V_{sw,e}}{V_{sw,c}}$, in real engines, is generally not too far from 1. In our analysis, instead, $\frac{V_{sw,e}}{V_{sw,c}} > 2$ was found.